ELSEVIER

Physica D 81 (1995) 177–203

PHYSICA D

Phase transitions in networks of chaotic elements with short and long range interactions

Jérôme Losson [a], John Milton [b,c], Michael C. Mackey [d]

[a] *Center for Nonlinear Dynamics and Department of Physics, McGill University, 3655 Drummond, Rm 1125, Montréal, Qué, H3G-1Y6 Canada*

[b] *Department of Neurology and Committee on Neurobiology, The University of Chicago Hospitals, MC 2030, 5841 South Maryland, Chicago, Il 60637, USA*

[c] *Center for Nonlinear Dynamics, McGill University, 3655 Drummond, Montréal, Qué, H3G-1Y6 Canada*

[d] *Center for Nonlinear Dynamics and Departments of Physiology, Physics, and Mathematics, McGill University, 3655 Drummond, Rm 1124, Montréal, Qué, H3G-1Y6 Canada*

Received 8 June 1994; revised 23 August 1994; accepted 28 September 1994
Communicated by K. Kaneko

Abstract

This paper investigates the statistical properties of networks of chaotic elements modeled by coupled map lattices. Transitions separating statistically stable and periodic phases are numerically observed in generic models of excitable media. Similar transitions are studied analytically in lattices of piecewise expanding maps by considering the spectral properties of the Perron–Frobenius operator using the theory of functions of bounded variation in $\mathbb{R}^n$.

1. Introduction

Models framed as coupled map lattices (CML) have been receiving increasing attention in the description of spatiotemporal dynamics. Typically, in two spatial dimensions, these CML's are of the form

$$x_{t+1}^{kl} = (1-\varepsilon)S(x_t^{kl}) + \frac{\varepsilon}{p}\sum_{\substack{p \text{ nearest} \\ \text{neighbors}}} S(x_t^{ij}), \quad \varepsilon \in (0,1), \tag{1}$$

where S describes the local dynamics. Periodic boundary conditions are imposed. When $p = 4$, the coupling in (1) is said to be diffusive, whereas when the p-neighbourhood encompasses all sites of the lattice, the coupling is referred to as mean field. Applications of CML's to the description of spatiotemporal dynamics range from the evolution of various ecosystems [39], to image processing algorithms [37], to the evolution of genetic sequences [10] and the interfacial dynamics in many reaction diffusion systems (cf. [26] and references therein). Some CML's tend to form large scale patterns, while others display spatiotemporal chaos, depending on the properties of the local transformation and on those of the inter-element coupling architecture.

SSDI 0167-2789(95)00203-7

This paper is concerned with the transitions which separate two distinct phases in these systems. It was shown in a previous study [27] that lattices of diffusively coupled chaotic unimodal maps exhibit two "phases": a spatiotemporally chaotic phase in which the statistical quantifiers can be computed with respect to a unique absolutely continuous invariant measure, and another phase characterized by the cyclical evolution of phase space densities. This asymptotically periodic phase reflects a cyclical spectral representation of the Perron–Frobenius operator induced by the lattice transformation, and is associated with the formation of large scale patterns when the local map is a generalized tent map. The presence of statistical cycling in coupled map lattices has been discussed in some detail by Chaté and Manneville (cf.. Section 3.2.2 of [7], and [8]) and by Gallas et al. [14], and Chaté and Manneville [6] in various cellular automata. In these references, the statistical cycling discussed here is sometimes referred to as "noisy periodicity".

Here we show that there is a class of biologically relevant CML's (referred to herein as excitable CML's) which generate large scale patterns when they are numerically observed to display statistical cycling. This observation is used to motivate an analytical study of asymptotic periodicity in CML's as a function of the inter-element coupling. Although it has been conjectured [18] that the formation of large scale patterns in CML's was a consequence of this statistical cycling, we show that this relationship holds only in the case of a linear coupling architecture and that even in this case asymptotic periodicity is a necessary, but not sufficient, condition for pattern formation.

In Section 2 we introduce excitable CML's and numerically investigate the relationship between their statistical properties and the appearance of patterns. The statistical cycling is discussed analytically in Section 3: the Perron–Frobenius operator induced by piecewise expanding CML's is investigated using the theory of functions of bounded variation. In Section 4, analytically tractable CML's with linear couplings which display the kind of cycling demonstrated in Section 2 are presented, and phase diagrams for these systems are obtained using the methods presented in Section 3. In Section 5, this analysis is extended to nonlinear coupling architectures.

2. Excitable CML's

A biologically motivated map which has surprisingly received relatively little attention in the study of coupled map lattices is the asymmetric bimodal map

$$x_{t+1} = \left(a + \frac{b}{G(x_t)}\right) x_t , \tag{2}$$

where $G(x) = 1 + x^n$ and $a + b > 1 > a > 0$. These maps arise in the description of the growth of ecological populations [3,9,31], neural networks [33], in the analysis of cardiac arrhythmias [38], and the study of the Belousov–Zhabotinsky chemical reaction [35]. They describe systems in which the dynamics depend on a threshold: rapid growth, or excitation, occurs when the variable crosses the threshold and is followed by a relatively long period of decline or decay. In this sense, these maps can be regarded as simple analogues for locally excitable dynamics. The bifurcation diagrams for these maps are quite complex and include stable limit cycles as well as regions of "banded" chaos [31].

To construct the CML it is necessary to derive the appropriate form of the coupling architecture. The coupling is most easily obtained in the setting of an ecosystem composed of k territories in which the local dynamics of the kth territory is described by (2). Eq. (2) has been used to describe the growth of certain territorial animal populations, such as the bobwhite quail, and describes a population which grows at rate $\sim (a + b)$ when $x < 1$ and declines at rate $\sim a$ when $x > 1$ [31]. The decrease in growth rate for large population densities arises because of competition between individuals once the population exceeds the number which can

be accommodated in preferred habitats. It follows that the influence of individuals in the $i \neq j$th territory on the jth territory must be through the term G, and hence the coupled map lattice is of the form

$$x_{t+1}^i = \left(a + \frac{b}{G^{(i)}(\boldsymbol{x}_t)}\right) x_t^i, \tag{3}$$

where $i = 1, \cdots, k$ is a space index which again need not be a scalar, and $\boldsymbol{x}_t = (x_t^i, \cdots, x_t^k)$ denotes the state of the lattice at time t. Franke and Yakubu [13] introduced a coupling scheme given by

$$G^{(i)}(\boldsymbol{x}_t) = 1 + \sum_{j=1}^{k} \left[x_t^j\right]^n$$

to describe globally coupled species of bobwhite quail competing for shared resources and showed that for sufficiently large n, the species in all territories except one became extinct.

More realistically the coupling should reflect the fact that the greater the distance between two territories, the smaller the interaction between them. We therefore define

$$G^{(i)}(\boldsymbol{x}_t) = 1 + \left[x_t^i + \sum_{j=1, \neq i}^{k} w_{ij} x_t^j\right]^n, \tag{4}$$

where w_{ij} denotes the weight of the connection between x_t^j and x_t^i. This weight should decrease as the distance $\mathrm{dist}(x^i, x^j)$ between sites x^i and x^j increases. The distance between sites is calculated using the Euclidean metric:

$$\begin{aligned}
&\mathrm{dist}(x^i, x^j) = |i - j| && \text{for dimensionality 1,}\\
&\mathrm{dist}(x^{i_1 i_2}, x^{j_1 j_2}) = \sqrt{(j_1 - i_1)^2 + (j_2 - i_2)^2} && \text{for dimensionality 2,}\\
&\text{etc.}
\end{aligned}$$

The simplest coupling architecture decreasing with distance is piecewise constant:

$$w_{ij} = \begin{cases} 1/\mathcal{N} & \text{if } \mathrm{dist}(x^i, x^j) \leq R, \\ 0 & \text{if } \mathrm{dist}(x^i, x^j) > R, \end{cases} \tag{5}$$

where $\mathcal{N}$ denotes the number of territories located within Euclidean distance R of x_t^i. In other words, the evolution of the local territory x^i is influenced in an inhibitory fashion by the mean activity in a surrounding sphere of radius R.

The inhibitory effect of the coupling in (5) is illustrated by the behavior of the map

$$S^{\xi}(z) = \left(a + \frac{b}{1 + (z + \xi)^n}\right) z \tag{6}$$

which is another way of writing (3) with coupling (4) [i.e. the sum in (4) is replaced by the constant factor ξ]. Fig. 1 illustrates the fact that if ξ is large, which represents a large mean activity in the neighbourhood of any lattice site x_t^i, the value x_{t+1}^i tends to be smaller than x_t^i. The growth of x_t^i is therefore inhibited locally by the activity of its neighbors.

The system (3) with (4) and (5) can now be investigated when the lattice is two dimensional for various coupling ranges R and control parameters. When the parameters are such that the local maps possess stable limit cycles, the whole lattice synchronizes and forms "coherent structures" whose stability properties have

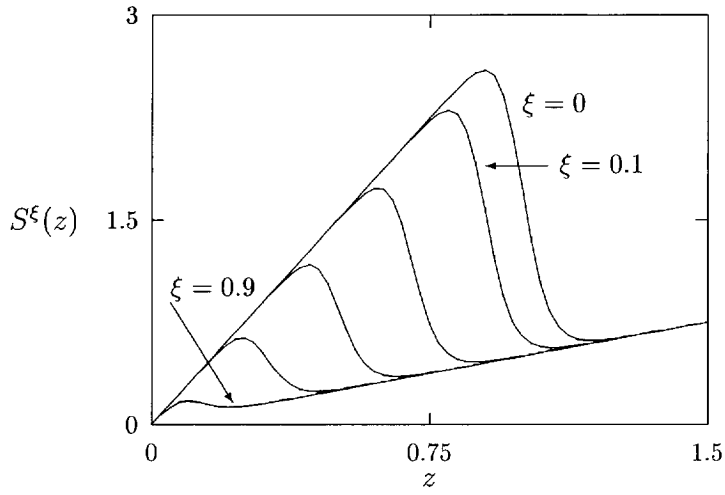

Fig. 1. Superimposition of several curves of the map (6) with $a = 0.5$, $b = 2.5$, $n = 29$ and $\xi = 0, \cdots, 0.9$.

been discussed previously in the context of diffusively coupled maps [1]. We do not consider these dynamics further here, but instead focus on the nontrivial statistical properties of the CML which arise when the local maps are chaotic.

When the local map is chaotic, numerical studies indicate that two distinct types of statistical evolutions are possible. Varying one (or several) control parameters can result in a transition from one phase to another (e.g. Fig. 3 displays one phase while Fig. 6 displays the other in the excitable CML presented above). For theoretical reasons developed in [27], these transitions are appropriately described as phase transitions since they involve qualitative changes in the thermodynamic state of the chaotic CML's under consideration (cf. the discussion related to the distribution of activity, below, and the introduction of Section 3).

Each phase is characterized by the behavior of various statistical quantifiers of the motion which evolve in qualitatively differing ways depending on the phase of the CML. There are many such quantifiers which have been developed to investigate spatiotemporal dynamics, and highlight nonlinear correlations between the elements (e.g. the mutual information), various stretching rates (e.g. the Lyapunov spectrum) or other information theoretic quantities of interest (e.g. the Rényi dimensions). In this section, we use simple quantifiers to characterize unambiguously the equilibrium statistical properties of system (3) with (4) and (5).

2.1. The distribution of activity

This quantity is the histogram of the activity on a large lattice at time t. It approximates the density F_t which is implicitly defined by the relation:

$$\langle x_t \rangle = \frac{1}{N^2} \sum_{k,l} x_t^{kl} F_t(x_t^{kl}), \tag{7}$$

where $\langle \cdot \rangle$ denotes the average activity of the quantity inside the brackets. If $F_t : \mathbb{R} \longmapsto \mathbb{R}$ does not reach a stable fixed point as the system evolves, then it can be shown that the phase space density $f_t : \mathbb{R}^{N^2} \longmapsto \mathbb{R}^{N^2}$ which describes the statistical properties of an ensemble of CML's (with N^2 sites) will also not reach a fixed point [27]. As discussed below, the CML's under consideration here can display a form of statistical behavior at equilibrium which is thought to reflect a cyclical spectral decomposition of the operator which governs the

evolution of f_t (the Perron–Frobenius operator). Therefore, it is of interest to compute F_t since it gives us an efficient description of the temporal behavior of f_t, the N^2-dimensional phase space density. Studying the evolution of f_t (or the more efficient F_t) provides a means to investigate the nonequilibrium thermodynamics of CML's, because the thermodynamic state of a CML with phase space $\mathbb{X}$ is the measure space $(\mathbb{X}, \mathcal{B}, \mu_t)$ where μ_t is associated here with a phase space density f_t, and $\mathcal{B}$ is an appropriately defined time-independent partition of $\mathbb{X}$ (i.e. a σ-algebra). Another statistical tool we use to investigate the dynamics of our CML's are the so-called linear correlation functions.

2.2. Linear correlation functions

These functions are defined for a trajectory $\{y_i\}_{i=1}^{Q}$ which is either the temporal evolution of a single site, or the activity along one spatial direction. Mathematically we have:

$$\rho(i) = \frac{c_i}{c_0}, \quad c_i = \frac{1}{Q}\sum_{j=1}^{Q-i}\left(y_j - \langle y\rangle\right)\left(y_{j+i} - \langle y\rangle\right). \tag{8}$$

2.3. The Boltzmann–Gibbs entropy

The Boltzmann–Gibbs entropy of a probability density f_t provides a measure of the difference between f_t and the uniform density. If f_t is the ensemble (or phase space) density of a dynamical system at time t, its Boltzmann–Gibbs entropy at time t takes the form:

$$H_t(f_t) = -\int_{\mathbb{X}} f_t \ln f_t \, d\boldsymbol{x}_t, \tag{9}$$

where $\mathbb{X}$ denotes the phase space. When large CML's are considered, obtaining f_t is computationally very costly. However, as mentioned above, some of the properties of f_t can be studied by focusing on the one dimensional function F_t, and therefore, the Boltzmann–Gibbs entropy discussed in Figs. 2 and 5 will be the entropy of F_t. For a detailed discussion of the relevance of the Boltzmann–Gibbs entropy to a discussion of the thermodynamics of chaotic dynamical systems, see [29].

Having briefly defined three statistical descriptors of CML dynamics, we are in a position to discuss the two distinct statistical phases displayed by system (3) with (4) and (5). The first is a reflection of the fact that the local map is probably ergodic (and perhaps even mixing). As shown in Fig. 2 the statistical quantifiers of the motion relax to steady states which reflect the probable existence of an invariant measure describing the equilibrium thermodynamic properties of the lattice. In this case, the activity of the lattice (cf. Fig. 3) is spatially as well as temporally chaotic. The resulting behavior has been termed "spatiotemporal chaos" [4,5,11,19] and was first proposed as an interesting paradigm to study fluid turbulence.

The second of the two phases mentioned above is characterized by the cyclical statistical behavior displayed in Fig. 4 and the possible formation of large scale patterns, examples of which are given in Fig. 5. It is conjectured here that this cyclical statistical behavior reflects the fact that the measures (and their densities) evolving under the action of the CML are not converging to a steady state, but to a stable limit cycle (in the space of probability densities). This in turn would be a consequence of the cyclical spectral decomposition of the Perron–Frobenius operator which governs the evolution of these densities. A property of the transfer operator known as asymptotic periodicity (defined rigorously in Section 4.1, and presented more intuitively in [27]) would account for such behavior, and will be analytically described for simpler CML's in Section 5.

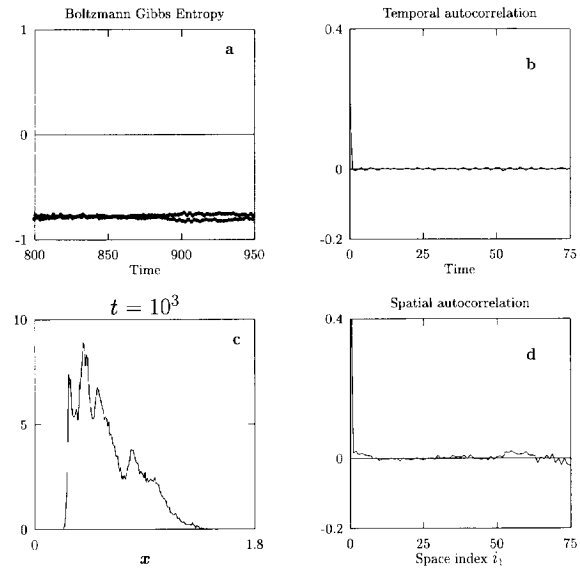

Fig. 2. Behavior of various statistical quantifiers of the dynamics of the CML (3) in dimension 2, with $N \times N$ elements and periodic boundary conditions ($N = 200$), and with R of Eq. (5) being 3. In all panels, the parameters are : $a = 0.65$, $b = 2.15$ $n = 45$. (a) Evolution of the Boltzmann–Gibbs entropy (9) of the density F_t displayed in (c) and defined in (7). (b) Behavior of the temporal autocorrelation function (8) at a "typical site" on the lattice. (c) The distribution of activity F_t across the lattice at equilibrium; this probability density is time invariant and probably reflects the existence of an invariant measure. It's invariance does not rigorously imply, but strongly indicates invariance of the measure in $\mathbb{R}^{N^2}$. (d) Spatial correlation function for the left panel of Fig. 3.

Fig. 3. These two panels are snapshots of the activity of a 200 × 200-element lattice with periodic boundary conditions at times $t = 10^3$ (left panel) and $t = 10^3 + 1$ (right panel). They display spatiotemporal chaos in the CML (3) with 200 × 200 sites. The parameters are as in Fig. 2. The initial distribution of sites was uniform over [0.5, 1.5].

The formation of large scale patterns occurred only in the statistically cycling regime. However, there is still no clear understanding of the possible link between statistical instability in this system and the formation of patterns.

When patterns appear, two scenarios can be observed: (1) synchronized clusters can grow in a relatively short time (less than 10^3 iteration for a lattice of $\mathcal{O}(10^4)$ elements) until they cover the entire lattice (as in the top panels of Fig. 6): The statistical cycling is then temporal rather than spatial [the synchronization within each cluster is not deterministic: all the sites within one cluster are contained within a small region of the real line sometimes referred to as a *band*, as in Fig. 4]; and (2) the expansion of the clusters is very slow,

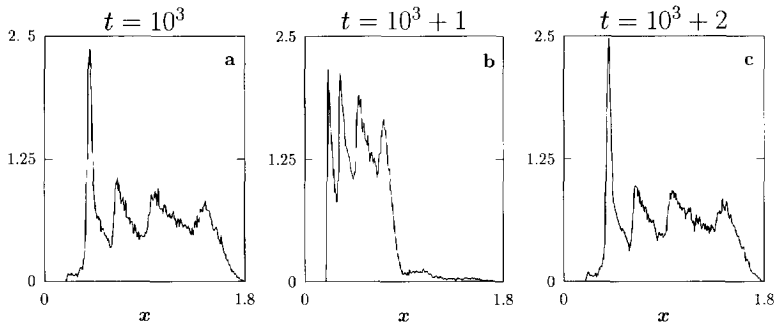

Fig. 4. Illustration of statistical cycling in the CML (3). The three panels display the distribution of activity (7) across a lattice at three consecutive times, when the lattice is composed of 200×200 sites, and the parameters are: $a = 0.5$, $b = 2.5$, $n = 18$. The initial distribution was uniform over $[0.5, 1.5]$. The exact asymptotic cycle (in density space) depends on the initial preparation (cf. Remark 1 in Section 3.1).

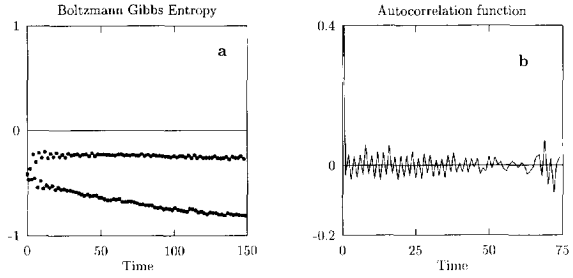

Fig. 5. The temporal correlation function (8) and Boltzmann Gibbs entropy (9) of F_t for the CML (3) when the parameters are the same as in Fig. 4. The "equilibrium" consists in two metastable states visited alternatively in time.

and during a very long transient, macroscopic clusters appear to be metastable. In this case, (bottom panels of Fig. 6), the statistical cycling is both temporal and spatial (the spatial cycling reflecting the presence of correlated and anticorrelated clusters of activity). In other words, the main difference between the situations which give rise to the formation of large clusters of correlated activity, and the situations which give rise to the synchronization of the entire lattice seems to be the length of transients: It appears that the patterns of Fig. 6 (bottom panels) eventually synchronize and look like those of Fig. 6 (top panels), but the transients are, as expected [21], extremely long.

Figs. 3 and 6 display snapshots of the activities of 200×200 lattices of maps of the form (3) coupled together according to (4) with (5), with periodic boundary conditions and for different values of the radius R and control parameters. In Figs. 2, 4 and 5, some of the standard statistical quantifiers of chaotic motion are displayed when the lattice is either in the statistically stable or the statistically periodic phase. It is important to realize that the regions of parameter space in which both statistical stability and statistical cycling are observed are "large" in the sense that they are easily located during preliminary numerical trials.

In summary, our numerical results indicate that:

(1) An initially featureless excitable CML can spontaneously organize itself into large clusters of correlated and anti-correlated activity (cf. Fig. 6).

(2) The formation of large scale patterns occurs only when the statistical behavior of the lattice is nontrivial. In this case the lattice does not relax to statistical equilibrium but it evolves to a statistically periodic state. This implies that the CML under consideration possesses a thermodynamic equilibrium unlike those described in classical statistical mechanics. This equilibrium consists in a sequence of states visited periodically in time.

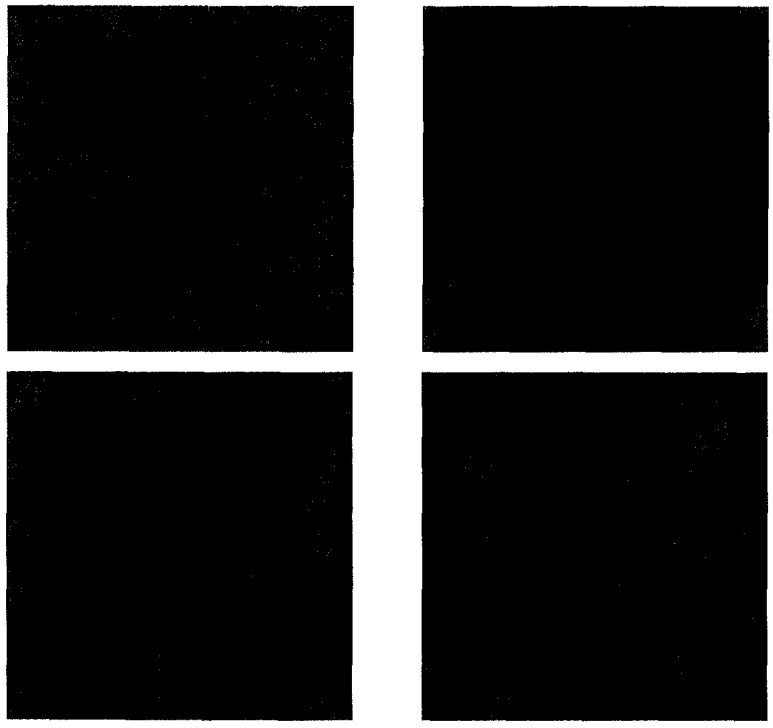

Fig. 6. Snapshots of the activity of a 200 × 200-site CML (3) when it is in the statistically cycling regime. Left panels: $t = 10^3$; Right panels: $t = 10^3 + 1$. The top panels illustrate the formation of correlated clusters of activity which cover the entire lattice. The parameters in this case are as in Figs. 4 and 5 with 82 nearest neighbors ($R = 5$) included in the neighbourhood. The bottom panels display the formation of patterns for the same parameter values but only 28 nearest neighbors ($R = 3$) influencing the activity of a given site. The initial preparations of the lattices were featureless, and the initial condition for each site was a random number picked from a density uniform on [0.5, 1.5].

We will come back to the implications of this observation in the discussion.

Given the paucity of rigorous results concerning the dynamics of large chaotic CML's, it is of great interest to describe this behavior analytically. Unfortunately, the map (3) cannot at present be dealt with in such a manner because it is not expanding everywhere. We propose in the next Section a nonlinear CML which accounts for much of the complexity described here, while remaining amenable to analytic treatment.

3. Thermodynamics of CML's

The statistical properties of coupled map lattices defined by the nonsingular mapping $\Phi : \mathbb{X} \longmapsto \mathbb{X}$ can be studied by investigating the spectral properties of the associated Perron–Frobenius operator $\mathcal{P}_\Phi : \mathrm{BV}(\mathbb{X}) \longmapsto \mathrm{BV}(\mathbb{X})$. $\mathrm{BV}(\mathbb{X})$ is the space of functions of bounded variation supported on $\mathbb{X}$ endowed with the bounded variation norm (for definitions, see [15]). The properties of $\mathrm{BV}(\mathbb{X})$ are relevant to our discussion of coupled map lattices, because the phase space probability densities which describe the ensemble properties of CML's are elements of $\mathrm{BV}(\mathbb{X})$. Note that $\mathrm{BV}(\mathbb{X})$ endowed with the bounded variation norm $\|\cdot\|_{\mathrm{BV}} = \|\cdot\|_{\mathrm{L}^1} + \bigvee(\cdot)$, where $\bigvee$ is the variation, is a Banach space (the proof makes use of the semi-continuity property of variation, and is given for $\mathbb{X} \subset \mathbb{R}^N$ in Remark 1.12 of [15]).

The evolution of the phase space densities is governed by a linear Markov operator known as the Perron–

Frobenius operator. The fixed points of this operator are the densities associated with invariant measures. In this paper, the Perron–Frobenius operator is defined on spaces of probability densities associated with absolutely continuous measures, though in general it can be defined to act directly on (noncontinuous) measures. This would be helpful to consider the statistical mechanics of dynamical systems such as cellular automata for example, but would bring unnecessary technical difficulties to the study of the coupled map lattices we are concerned with. The convergence properties of sequences of densities evolving under the action of the Perron–Frobenius operator describe the nonequilibrium statistical properties of the systems under consideration. In this sense, the Perron–Frobenius operator offers a description of coupled map lattices analogous to the probabilistic description of ordinary differential equations by Liouville's equation, or the description of density evolution under the action of Langevin's equation by the Fokker–Planck equation.

3.1. Mathematical preliminaries

A general introduction to the Perron–Frobenius operator $\mathcal{P}_\Phi$ is given in [25], and the usefulness of this operator to investigate the thermodynamics of chaotic systems is discussed in [2]. For piecewise monotone transformations and for any f_t in $\mathrm{BV}(\mathbb{X})$,

$$\mathcal{P}_\Phi f_t(x) = \sum_{y\in\Phi^{-1}(x)} \frac{f_t(y)}{\mathcal{J}(\Phi(y))} = f_{t+1}(x). \tag{10}$$

Explicitly, let $\Phi_{|\pi_i}$ denote the strictly monotonic restriction of Φ to the ith of m sets π_i, such that $\bigcup_i \pi_i = \mathbb{X}$, and let $\tilde{\pi}_i = \Phi_{|\pi_i}(\pi_i)$. Then, (10) can be written as

$$\mathcal{P}_\Phi f_t(x) = \sum_{i=1}^{m} \frac{f_t(\Phi_{|\pi_i}^{-1}(x))}{\mathcal{J}_i^{-1}(x)} \chi_{\tilde{\pi}_i}(x)\,, \tag{11}$$

where $\chi_{\tilde{\pi}_i}(x) = 1$ if $x \in \tilde{\pi}_i$, 0 otherwise, and

$$\mathcal{J}_i^{-1}(x) = |\det D\Phi_{|\pi_i}^{-1}(x)| \tag{12}$$

is the absolute value of the Jacobian of $\Phi_{|\pi_i}^{-1}(x)$.

Let $f_t = \mathcal{P}_\Phi^t f_0$, $t = 1, \cdots$ denote the iterates under $\mathcal{P}_\Phi$ of an initial density $f_0 \in \mathrm{BV}(\mathbb{X})$. The convergence properties [25] of the sequence of functions $\{f_n\}$, reflects the thermodynamic properties of Φ. For example, Φ is ergodic if and only if there exists an invariant density f_* such that $\mathcal{P}_\Phi f_* = f_*$ and that the sequence is *weak Cesàro convergent* to $f_*(x)$, for all probability densities f_0:

$$\lim_{t\to\infty} \frac{1}{t} \sum_{k=1}^{t} \int_{\mathbb{X}} f_k(x) q(x) dx = \int_{\mathbb{X}} f_*(x)\, q(x)\, dx, \quad \text{for all } q \in \mathrm{BV}(\mathbb{X}).$$

A stronger (but familiar) property, mixing, is equivalent to the *weak convergence* of the sequence to the invariant density:

$$\lim_{t\to\infty} \int_{\mathbb{X}} f_t(x)\, q(x)\, dx = \int_{\mathbb{X}} f_*(x)\, q(x)\, dx, \quad \text{for all } q \in \mathrm{BV}(\mathbb{X}),$$

for all probability densities f_0. In this paper, we will consider situations in which the sequence of phase space densities evolves to a periodic cycle, reflecting a property of $\mathcal{P}_\Phi$ known as asymptotic periodicity. Asymptotic periodicity is a property of certain linear Markov operators, and is described in detail in [23,24].

Definition 1. Asymptotic periodicity. $\mathcal{P}_\Phi$ is asymptotically periodic if there exist finitely many distinct probability density functions $g_1, \cdots, g_r$ with disjoint supports, a unique permutation γ of the set $\{1, \cdots, r\}$ and positive linear continuous functionals $\Gamma_1, \cdots, \Gamma_r$ on $\mathrm{BV}(\mathbb{X})$ such that

$$\lim_{t\to\infty} \left\| \mathcal{P}_\Phi^t \left(f_0 - \sum_{i=1}^{r} \Gamma_i[f_0] g_i \right) \right\|_{\mathrm{L}^1} = 0 \tag{13}$$

and

$$\mathcal{P}_\Phi g_i = g_{\gamma(i)}, \quad i = 1, \cdots, r.$$

If $\mathcal{P}_\Phi$ satisfies these conditions with $r = 1$, it is usually said to be *asymptotically stable*, a special case of asymptotic periodicity, which implies mixing and the decay of correlations. If the permutation γ is circular, asymptotic periodicity implies ergodicity. For an intuitive discussion of asymptotically periodic systems the reader is referred to [25]. It is enough to note here that in such systems there exists an invariant density which is almost never observed. Instead, the evolution of phase space densities is time periodic (in the asymptotic regime), and so is the evolution of all statistical quantifiers of the motion which are computed with respect to this invariant density (thermodynamic entropies, correlation functions etc.).

Remark 2. It is important to note the dependence of the functionals Γ_i on the initial density f_0. This implies a dependence on initial conditions for asymptotically periodic systems which is different, and to some extent much stronger, than that usually associated with chaotic dynamics: here the *ensemble* properties of a given CML depend on the initial ensemble. There is no rigorous study of the sensitivity of these functionals on variations of the initial density, but numerical investigations indicate that it is common to observe cycles with very different weighting of the g_i components for apparently similar initial densities.

In general it is necessary to resort to numerical simulations to demonstrate the presence of asymptotic periodicity in a coupled map lattice. However, as we show in Section 3.2, it is possible to derive sufficient conditions for asymptotic periodicity in the special case that Φ is piecewise linear.

With these preliminary definitions, it is possible to investigate the evolution of phase space densities under the action of certain CML's.

3.2. *Sufficient conditions for statistical cycling*

Here we derive a sufficient condition for the asymptotic periodicity of the Perron–Frobenius operator $\mathcal{P}_\Phi$ for coupled map lattices composed of piecewise expanding mappings. Our approach, inspired by the work of Góra and Boyarski [16], involves placing bounds on the variation of $\mathcal{P}_\Phi f$, and then using these bounds to invoke a basic result from the theory of linear operators due to Ionescu–Tulcea and Marinescu [40]. Their result is formal, but in our case (i.e. by considering an operator acting on elements of $\mathrm{BV}(\mathbb{X})$) it implies that if $\bigvee(\mathcal{P}_\Phi f)$ is such that

$$\bigvee(\mathcal{P}_\Phi f) \leq \omega \bigvee(f) + \Omega, \tag{14}$$

where $0 < \omega < 1$ and $\Omega > 0$, then $\mathcal{P}_\Phi$ is asymptotically periodic. It should be noted that the above provides a sufficient condition for the spectral decomposition (13), and that when condition (14) is not satisfied, we are not in a position to discuss the density evolution associated with chaotic CML's.

For typical CML's, the requirement that (14) be satisfied places natural constraints on the control parameters of Φ. To proceed, note that since Φ is a piecewise monotone mapping we have from (11)

$$\begin{aligned}\bigvee(\mathcal{P}_\Phi f) &= \bigvee\left(\sum_{i=1}^{m}\frac{f(\Phi^{-1}_{|\pi_i}(x))}{\mathcal{J}_i^{-1}(x)}\chi_{\tilde{\pi}_i}(x)\right)\\ &\le \sum_{i=1}^{m}\bigvee\left(\frac{f(\Phi^{-1}_{|\pi_i}(x))}{\mathcal{J}_i^{-1}(x)}\chi_{\tilde{\pi}_i}(x)\right)\\ &\le \mathcal{Q}\sum_{i=1}^{m}\bigvee\left(f(\Phi^{-1}_{|\pi_i}(x))\chi_{\tilde{\pi}_i}(x)\right),\end{aligned} \tag{15}$$

where $\mathcal{Q}\in\mathbb{R}^+$ satisfies

$$\frac{1}{\max_{\pi_i\in\Pi}\mathcal{J}_i^{-1}(x)} \ll \mathcal{Q} \ll \frac{1}{\min_{\pi_i\in\Pi}\mathcal{J}_i^{-1}(x)} \tag{16}$$

and depends on the transformation under consideration. Eq. (15) can be further simplified using example 2.14 of [15]:

$$\begin{aligned}\bigvee\left(f(\Phi^{-1}_{|\pi_i}(x))\chi_{\tilde{\pi}_i}(x)\right) &\le \bigvee\left(f(\Phi^{-1}_{|\pi_i}(x))\right)\Big|_{x\in\tilde{\pi}_i} + \int_{\mathbb{X}}|f(\Phi^{-1}_{|\pi_i}(x))\nabla_{\mathrm{d}}\chi_{\tilde{\pi}_i}|d\mu_{\mathrm{L}}(N)\\ &= \bigvee\left(f(\Phi^{-1}_{|\pi_i}(x))\right)\Big|_{x\in\tilde{\pi}_i} + \int_{\partial\tilde{\pi}_i}|\,f(\Phi^{-1}_{|\pi_i}(x))\,|\,d\mu_{\mathrm{L}}(N-1),\end{aligned} \tag{17}$$

where $\mu_{\mathrm{L}}(N)$ denotes the Lebesgue measure in $\mathbb{R}^N$. Intuitively, if $u\in\mathrm{BV}(\mathbb{X})$, the integral of $|u|$ over the boundaries of subsets of $\mathbb{X}$ must depend on the geometry of these boundaries. In fact, from Lemma 3 of [16] we have

$$\int_{\partial\tilde{\pi}_i}u(x)\,d\mu_{\mathrm{L}}(N-1) \le \frac{1}{\sin\theta(\tilde{\pi})}\bigvee(u(x))\Big|_{x\in\tilde{\pi}_i} + \mathcal{K}_{\tilde{\pi}_i}, \tag{18}$$

where $\mathcal{K}_{\tilde{\pi}_i}>0$ is bounded and $\sin\theta(\tilde{\pi})$ depends on the geometry of $\tilde{\pi}_i$: $\theta(\tilde{\pi})$ is an angle, defined in Appendix A, which depends on the minimum angle of intersection of any two faces $\partial\tilde{\pi}_i$.

Calculating $\sin\theta(\tilde{\pi})$ is tedious but straightforward when the $\tilde{\pi}_i$'s are bounded by hyperplanes such that the edges of $\partial\tilde{\pi}_i$ intersecting at a vertex do so at angle θ [a detailed calculation of $\sin\theta(\tilde{\pi})$ is presented in Appendix A for various cases of interest]. Letting $\mathcal{K}=\max_i\mathcal{K}_{\tilde{\pi}_i}$, and applying (18) with $u(x)=f(\Phi^{-1}_{|\pi_i}(x))$, (17) becomes

$$\begin{aligned}\bigvee\left(f(\Phi^{-1}_{|\pi_i}(x))\chi_{\tilde{\pi}_i}(x)\right) &\le \bigvee\left(f(\Phi^{-1}_{|\pi_i}(x))\right)\Big|_{x\in\tilde{\pi}_i} + \frac{1}{\sin\theta(\tilde{\pi})}\bigvee\left(f(\Phi^{-1}_{|\pi_i}(x))\right)\Big|_{x\in\tilde{\pi}_i} + \mathcal{K}_{\tilde{\pi}_i}\\ &= \bigvee\left(f(\Phi^{-1}_{|\pi_i}(x))\right)\Big|_{x\in\tilde{\pi}_i}\left[1+\frac{1}{\sin\theta(\tilde{\pi})}\right] + \mathcal{K}.\end{aligned} \tag{19}$$

A straightforward change of variables yields (when $\mathcal{J}_i(x)$ is independent of x, which is the case in the systems considered here)

$$\bigvee\left(f(\Phi^{-1}_{|\pi_i}(x))\right)\Big|_{x\in\tilde{\pi}_i} = \mathcal{J}_i\bigvee(f(x))\Big|_{x\in\pi_i} \le \mathcal{Q}\bigvee(f(x))\Big|_{x\in\pi_i}.$$

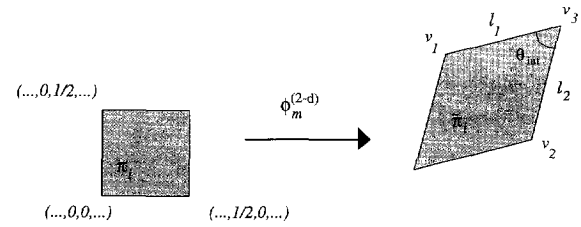

Fig. 7. Schematic diagram of the evolution of one of the hyperplanes bounding the set π_i under the action of the CML transformation Φ. As in the text, $\tilde{\pi}_i = \Phi_{|\pi_i}(\pi_i)$.

Summing the terms like (19) in (15), we obtain the inequality

$$\bigvee(\mathcal{P}_\Phi f) \leq \mathcal{Q}^2 \left[1 + \frac{1}{\sin\theta(\tilde{\pi})}\right] \bigvee(f) + m\mathcal{Q}^2\mathcal{K}, \tag{20}$$

which yields a method for determining the constants in (14). Therefore, if

$$\omega \equiv \mathcal{Q}^2 \left[1 + \frac{1}{\sin\theta(\tilde{\pi})}\right] < 1, \tag{21}$$

the theorem of Ionescu-Tulcea and Marinescu guarantees that $\mathcal{P}_\Phi$ is asymptotically periodic since $\Omega = m\mathcal{Q}^2\mathcal{K} > 0$.

4. Linear coupling

The association of large scale patterns and asymptotic periodicity in CML's was first observed for the case of a diffusively coupled CML in which the local transformation, S, is the generalized tent map [27]

$$S(z) = \min_{z\in[0,1]}\{az, a(1-z)\}, \quad a \in (1,2]. \tag{22}$$

Here we use the results of Section 3.2 to study asymptotic periodicity in lattice transformations of the form (1), with S given by (22) for various linear coupling architectures. This study is facilitated by the fact that for this choice of S, $\sin\theta(\tilde{\pi})$, and $\mathcal{Q}$ of condition (21) can be readily calculated.

4.1. *Calculating* $\sin\theta(\tilde{\pi})$

The phase space $\mathbb{X}$ of the transformation Φ is the direct product $\mathbb{X} = [0,1]^N$ if there are N sites on the lattice. Note that each of the elements of this product can be divided into two subintervals $I_1 = [0,1/2)$, $I_2 = [1/2,1]$ such that on each of these, S is monotone. Therefore the partition Π on which Φ is piecewise monotone contains 2^N sets, each one of which is of the form: $\pi_i = I_1^i I_2^{N-i}$, where $i = 1,\cdots,2^N$. In addition, note that Π is a rectangular partition since I_1 and I_2 are the same for all sites on the lattice.

As illustrated in Fig. 7, the "image sets" denoted $\tilde{\pi}_i$ $(i = 1,\cdots,m)$ are rhomboids (cf. [28]) whose edges subtend angles which are bounded away from 0. The smallest of these angles is denoted θ_{int}, and can be calculated explicitly by noting that the two dimensional restriction of the CML transformation Φ to the plane (x^i, x^j) (x^i and x^j belonging to the same p-neighbourhood) is

$$\Phi^{(2-d)}(\boldsymbol{x}_t) = \begin{cases} x^i_{t+1} = (1-\varepsilon)S(x^i_t) + \dfrac{\varepsilon}{p}S(x^j_t) + C_1, \\ x^j_{t+1} = (1-\varepsilon)S(x^j_t) + \dfrac{\varepsilon a}{p}S(x^i_t) + C_2, \end{cases}$$

where C_1 and C_2 depend only on the activity in the p-neighbourhood of the sites i and j (excluding x^i and x^j themselves). Hence,

$$\Phi^{(2-d)}(\cdots, 0, 1/2, \cdots) = \left(\cdots, \frac{\varepsilon a}{2p} + C_1, (1-\varepsilon)\frac{a}{2} + C_2, \cdots\right) \equiv v_1\,,$$

$$\Phi^{(2-d)}(\cdots, 1/2, 0, \cdots) = \left(\cdots, (1-\varepsilon)\frac{a}{2} + C_1, \frac{\varepsilon a}{2p} + C_2, \cdots\right) \equiv v_2\,,$$

$$\Phi^{(2-d)}(\cdots, 1/2, 1/2, \cdots) = \left(\cdots, \frac{a}{2} + \frac{a\varepsilon}{2}\left(\frac{1-p}{p}\right) + C_1, \frac{a}{2} + \frac{a\varepsilon}{2}\left(\frac{1-p}{p}\right) + C_2, \cdots\right) \equiv v_3\,.$$

Denote by ℓ_1 the edge linking v_1 to v_3 and ℓ_2 the edge linking v_2 to v_3. The slope of ℓ_1 is therefore $\varepsilon/p(1-\varepsilon)$, and the angle θ_{int} of intersection of ℓ_1 and ℓ_2 satisfies

$$\tan\theta_{\text{int}} = \frac{p(1-\varepsilon)[\varepsilon^2 - p^2(1-\varepsilon)^2]}{\varepsilon[\varepsilon^2 + p^2(1-\varepsilon)^2]}\,. \tag{23}$$

As shown in Appendix A this implies

$$\sin\theta(\tilde{\pi}) = \sqrt{\frac{1-\cos\theta_{\text{int}}}{N[1+(N-2)\cos\theta_{\text{int}}]}}\,, \tag{24}$$

where N denotes the number of elements on the CML under consideration (this number is N^2, and not N, for the systems investigated in the phase diagrams, cf. Figs. 8, 9 and 11)

4.2. Calculating $\mathcal{Q}$

If the tent maps (22) are coupled as in (1), the possible entries in the derivative matrix $D\Phi_{|\pi_i}$, are,

	$x^{kl} \in I_1$	$x^{kl} \in I_2$
$\phi'_{i,kk}(\boldsymbol{x})$	$(1-\varepsilon)a$	$-(1-\varepsilon)a$
$\phi'_{i,kl}(\boldsymbol{x})$	$(\varepsilon/p)a$	$-(\varepsilon/p)a$.

The absolute value of the determinant of this matrix remains unchanged when entire columns are multiplied by -1, and so

$$|\det D\Phi_{|\pi_i}| = \det|D\Phi_{|\pi_i}| = \det|D\Phi|,$$

where $|D\Phi|$ is a real matrix, whose diagonal entries are $(1-\varepsilon)a$, and nonzero off-diagonal entries are $(\varepsilon/p)a$. Since periodic boundary conditions are assumed, $|D\Phi|$ is also symmetric, and hence diagonalizable, and

$$\det|D\Phi| = \prod_{k=0}^{N-1}\lambda_k\,,$$

where the λ_k's are the eigenvalues of $|D\Phi|$. Although these eigenvalues depend on the coupling architecture, they are independent of both i and $\boldsymbol{x}$ when the map is piecewise linear with a slope whose absolute value is

constant on the phase space. Therefore $\det|D\Phi_{|\pi_i}|$ is also independent of x and i, and if there are N elements on the lattice

$$\mathcal{J}_i^{-1}(x) = \prod_{k=0}^{N-1} \lambda_k^{-1}, \quad \forall i = 1, \cdots, 2^N, \ \forall x \in \mathbb{X}, \tag{25}$$

where the expressions for the λ_k's for several coupling schemes are listed in Table 1 below. Recall that $\mathcal{Q}$ was defined implicitly in (15) by the requirement

$$\sum_{i=1}^{m} \bigvee \left(\frac{f(\Phi_{|\pi_i}^{-1}(x))}{\mathcal{J}_i^{-1}(x))} \chi_{\tilde{\pi}_i}(x) \right) \leq \mathcal{Q} \sum_{i=1}^{m} \bigvee \left(f(\Phi_{|\pi_i}^{-1}(x)) \chi_{\tilde{\pi}_i}(x) \right).$$

It is clear from (25) that

$$\sum_{i=1}^{m} \bigvee \left(\frac{f(\Phi_{|\pi_i}^{-1}(x))}{\mathcal{J}_i^{-1}(x))} \chi_{\tilde{\pi}_i}(x) \right) = \frac{1}{\prod_{k=0}^{N-1} \lambda_k^{-1}} \sum_{i=1}^{m} \bigvee \left(f(\Phi_{|\pi_i}^{-1}(x)) \chi_{\tilde{\pi}_i}(x) \right),$$

so it is natural to pick

$$\mathcal{Q} = \prod_{k=0}^{N-1} \lambda_k. \tag{26}$$

As a result, condition (21) for asymptotic periodicity, applied to a lattice of generalized tent maps (22) coupled linearly as in (1) becomes, if there are N elements on the lattice [note here that the phase diagrams of Figs. 8, 9 and 11 are given for lattices which possess N^2 elements]

$$\left[\prod_{k=0}^{N-1} \lambda_k^2 \right] \left[1 + \frac{1}{\sin\theta(\tilde{\pi})} \right] < 1. \tag{27}$$

Exact expressions for the eigenvalues are necessary to obtain concrete conditions on the parameters a, p and ε such that (27) holds. The periodic boundary conditions we have chosen are helpful in this regard since they ensure that the matrix $|D\Phi|$ is circular: the second row is obtained by shifting all the elements of the first row to the right by one position, so that if the entries of the matrix $|D\Phi|$ are denoted ϕ'_{kl} $(k, l = 1, \cdots, N)$ $\phi'_{kl} = \phi'_{(k+1)(l+1) \bmod N}$ (the modulo operator is a consequence of the periodic boundary conditions). For such matrices, [which are, again, associated with CML's with N elements] it is well known [32] that

$$\lambda_k = \sum_{m=1}^{N} \phi'_{1m} \, \mathrm{e}^{2\pi k m/N}, \quad k = 0, \cdots, N-1. \tag{28}$$

The table below gives explicit formulae for (28) for an $N \times N$ lattice of tent maps (so that k of (28) now runs from 0 to $N^2 - 1$) with several coupling architectures discussed in the literature:

The sum in the p nearest neighbors case is over half the sites which are included in the neighbourhood because each term in the sum arises from the contribution of two sites: x^m and its mirror image relative to the center of the neighbourhood. The exact expressions for the bounds of this sum are easily derivable, but cumbersome, and therefore not shown here explicitly (the sum is evaluated below, in Eq. (33) for the $p = 28$ case).

Table 1
Table of the eigenvalues of the derivative matrix $D\Phi$ associated with a square lattice of tent maps for various coupling architectures

Coupling	λ_k
diffusive	$(1-\varepsilon)a + \frac{1}{4}\varepsilon a\left[\cos\left(2\pi k/N^2\right) + \cos\left(2\pi/N\right)\right]$
p nearest neighbors	$(1-\varepsilon)a + \frac{2a\varepsilon}{p}\left[\sum_{m:p/2\text{sites}} \cos\left(\frac{2\pi k}{N^2}m\right)\right]$
mean field	$\left[1 - N^2\varepsilon/\left(N^2-1\right)\right]a$

Until now, no claim has been made concerning the period of the density cycle resulting from the cyclical spectral decomposition (13): there are no general results available to determine the quantity r in (13) (indicating the number of disjoint supports of the invariant density) and therefore providing a lower bound on the period of the density cycle (the upper bound being naturally $r!$). However, it is well established [41] that the tent map (22) displays a period doubling scenario in the evolution of densities, which can be summarized as follows:

$$2^{1/2^{n+1}} < a \leq 2^{1/2^n} \Longleftrightarrow \text{asymptotic periodicity of period } 2^n, \quad n = 0, 1, 2, \cdots. \tag{29}$$

A generalization of this result was derived for two diffusively coupled tent maps, and a phase diagram in the (a, ε) plane is given in [28] showing that the cascade behavior can be analytically investigated when two tent maps are coupled together. It is of interest to understand how this picture survives in arbitrarily large lattices of tent maps coupled together through various coupling schemes.

To carry out this analysis, we apply the formalism presented in Section 4 to compositions of the lattice transformation Φ with itself. Denote by Φ^n the transformation Φ composed n times with itself (i.e. $\Phi^2 = \Phi \circ \Phi$). If the spectral decomposition (13) applies to Φ^2 with $r = r_2 \neq 1$, then it necessarily applies to Φ with $r = r_1$, where $r_1 = 2r_2$. The same reasoning holds for higher order iterates of Φ and yields $r_1 = nr_n$ for Φ^n. We therefore investigate the spectral characteristics of the Perron–Frobenius operator associated with Φ^2, Φ^4 etc.

4.3. Diffusive coupling

Note that if λ_k is an eigenvalue of the transformation Φ, then λ_k^n is an eigenvalue of Φ^n, and so condition (27) for a lattice with N sites takes the form

$$\left[\prod_{k=0}^{N-1} \lambda_k^{2n}\right]\left[1 + \frac{1}{\sin\theta(\tilde{\pi})}\right] < 1 \tag{30}$$

with $\sin\theta(\tilde{\pi})$ given in (24). Fig. 8 examines the behavior of condition (30) for various iterates of Φ : Φ^2, Φ^4 and Φ^8. For clarity, Fig. 8 does not display the results of our analysis applied to Φ^n for $n > 8$, because the subsequent curves behave as expected. This phase diagram therefore generalizes previously published results [28] on two diffusively coupled tent maps to N dimensions. It should be clear that the curves displayed in Fig. 8 do not indicate precisely the location in the (a, ε) plane at which the spectral decomposition of the Perron–Frobenius operator changes. Instead, these curves indicate locations in parameter space at which *sufficient conditions* for a given spectral decomposition of $\mathcal{P}_\Phi$ change. This "onion" like structure is consistent with numerical investigations of diffusively coupled tent map lattices reported in [27], and indicates that the one-dimensional picture (29) essentially survives diffusive coupling, modulo some expected dependence on the coupling strength between the elements.

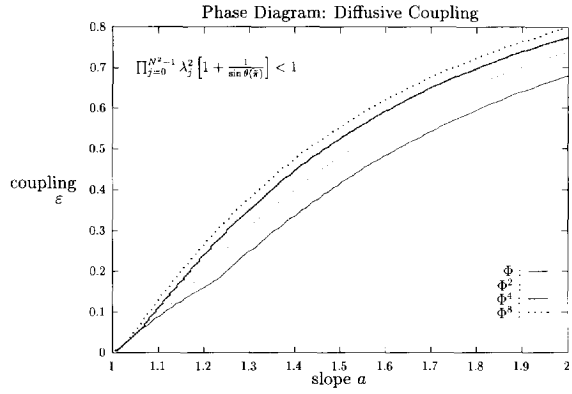

Fig. 8. Phase diagram for the diffusively coupled tent map with periodic boundary conditions. This figure was obtained from the condition (27) for a lattice of 200 × 200 elements, and eigenvalues corresponding to Φ, Φ^2, etc..

4.4. Mean field coupling

In this case, the evolution of every local site is influenced by the mean activity of the entire lattice. This coupling is of interest because it is a limiting case of long range couplings which are known to arise in optics (cf. [22] and references therein), in the study of evolutionary dynamics [12], and in many physical models of spatially extended systems [30]. The eigenvalues of the derivative matrix in this case are given in Table 1, and the condition (21) can again be evaluated explicitly. In this case, the simplicity of the eigenvalues (cf. Table 1) allows to go one step further since if N is large, we have

$$\lambda_k \sim (1-\varepsilon)a.$$

In addition, if there are N^2 sites on a lattice of globally coupled tent maps, and N is large, the results of Appendix A indicate that

$$\sin\theta(\tilde{\pi}) \sim N^{-2}.$$

Hence, condition (21) becomes

$$[1+N^2]\left[(1-\varepsilon)^2a^2\right]^{N^2} < 1,$$

which can be written

$$(1-\varepsilon)a < N^{(-1/N^2)}.$$

But $\lim_{N\to\infty} N^{(-1/N^2)} = 1$ (if $N = 200$ for example, $N^{(-1/N^2)} \simeq 0.9998675505$), so the condition (21) for a large lattice becomes effectively

$$(1-\varepsilon)a < 1.$$

Note also that $\lim_{N\to\infty} N^{(-1/nN^2)} = 1$ for $n > 1$, so that we do not expect the "onion-like" structure displayed in Fig. 8 to hold when the coupling is mean field.

Fig. 9 displays the phase diagrams for the globally coupled tent map lattice. This phase diagram is the analytic version of some early numerical results published by Kaneko on a similar model [22]. The overall shape of the transition curve published in that reference separating "spatiotemporal chaos" (or turbulence) and statistical cycling is in agreement with our analytic result, although systematic shifts in parameter space are clearly present.

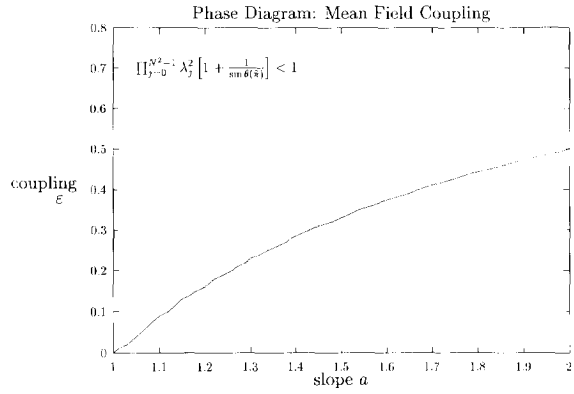

Fig. 9. Phase diagram for the globally coupled tent map lattice. The diagram is obtained by applying condition (27) with the eigenvalues of Table 1 corresponding to mean field coupling. It should be noted that the diagrams for Φ^n, $n = 2, 4, \cdots$, yield the *same* curve as the one displayed here. As explained in the text, this curve is accurately described by the function $\varepsilon = 1 - 1/a$.

This shift is most important for low values of the coupling ($\varepsilon \lesssim 0.3$) because in these cases, our estimates of the quantity $\mathcal{Q}$ are too conservative. The smaller shifts observed for high coupling values are probably due to a combination of transient effects (which render accurate numerical simulations computationally very costly) and inaccuracies in the various bounds of condition (21). In any case, the presence of such discrepancies is not surprising given the fact that the estimates given here for the phase transition curves correspond to changes in *sufficient* conditions for asymptotic periodicity, rather than changes in necessary *and* sufficient conditions.

The most common linear coupling architectures discussed in the literature, diffusive and mean field coupling, have now been treated analytically in a lattice of tent maps. We next investigate a coupling which is closer in nature to the competing populations model presented in Section 3.

5. Nonlinear coupling

The methods of Section 4 can be extended to more general systems in which the the neighbourhood of a given site acts on its evolution *via* a nonlinear coupling mechanism. Such mechanisms were illustrated in Section 2 when considering a generic model of excitable media with local inhibition. We now construct similar CML's which remain analytically tractable.

5.1. Coupled bimodal maps

As an example, consider a lattice transformation of piecewise linear maps coupled in a nonlinear fashion to mimic the inter-element inhibition of the excitable CML of Section 2:

$$\Phi^{(i)}(x_t) = (1-\varepsilon)S^{(i)}(x_t) + \frac{\varepsilon}{p}\sum_{\substack{p \text{ nearest} \\ \text{neighbors}}} S^{(j)}(x_t).$$

In this section, p is chosen so that the inter-element coupling is diffusive; i.e. $p = 2$ in dimension 1, $p = 4$ in dimension 2, etc.] The inhibitory effect of the neighbourhood is modeled by the local transformation:

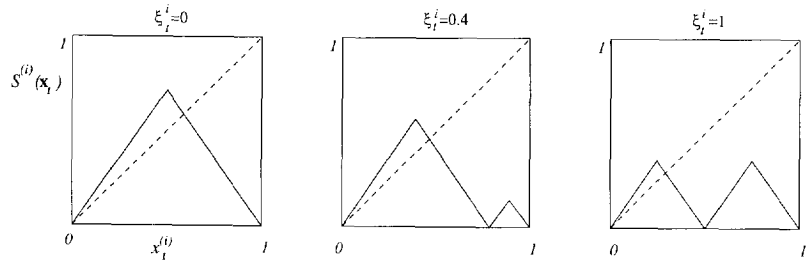

Fig. 10. Schematic diagram of the bimodal tent map of Section 5.1. The maximum activity of the map decreases if the mean activity of the neighbourhood ξ increases. This inter-element inhibition is meant to mimic the same feature in the more realistic model of Section 2.

$$S^{(i)}(x_t) = \begin{cases} ax_t^{(i)} & \text{if } x_t^{(i)} \in [0, \tau_t^i), \\ a(2\tau_t^i - x_t^{(i)}) & \text{if } x_t^{(i)} \in [\tau_t^i, 2\tau_t^i), \\ a(-2\tau_t^i + x_t^{(i)}) & \text{if } x_t^{(i)} \in [2\tau_t^i, \tau_t^i + 1/2), \\ a(1 - x_t^{(i)}) & \text{if } x_t^{(i)} \in [\tau_t^i + 1/2, 1], \end{cases} \tag{31}$$

where $\tau_t^i \in [1/4, 1/2]$ depends on the mean activity ξ_t^i in a neighbourhood of x_t^i:

$$\tau_t^i \equiv \frac{1}{2} - \frac{1}{4d} \sum_{\substack{d \text{ nearest} \\ \text{neighbors}}} x_t^j. \tag{32}$$

This nonlinear coupling is chosen so an increase in the sum over the d neighbors has an inhibitory effect on x_{t+1}^i. When S of CML (1) is given by (31), the transformation possesses two statistical regimes like the excitable CML discussed in Section 2. In one phase, the system seems to be ergodic, possessing a unique invariant measure, a one dimensional projection of which is observed numerically. In the other, the statistical quantifiers presented in Section 2 oscillate periodically in time, indicating that the Perron–Frobenius operator might be asymptotically periodic.

The qualitative observations made concerning the two possible statistical evolutions (to a steady state, or to a limit cycle) of the excitable CML (3) hold for the system (1) with (31). The details of the density cycles are obviously not the same for the two systems, and the structure of the maps is also very different. However, they have similar nonlinear inter-element coupling, and since we have only analytically investigated the behavior of CML's in which the coupling was linear, it is of interest to generalize this analysis to nonlinearly coupled CML's.

The analysis of the previous section can be completely carried out to yield conditions on the parameters of (31) sufficient for the cyclical spectral representation of the Perron–Frobenius operator. The eigenvalues of its derivative matrix cannot be evaluated explicitly as a function of the slope a and the number of neighbors p and d included in the two relevant neighborhoods. However, it it possible to derive upper and lower bounds on the quantity $\mathcal{Q}$ of condition (21) for (31).

5.2. Calculating $\mathcal{Q}$

If the d-neighbourhood includes all the sites located within Euclidean distance 3 of the site x_t^i (there are 28 such neighbors in dimension 2), $\mathcal{Q}$ satisfies:

$$\min(\mathcal{Q}_1, \mathcal{Q}_2) \leq \mathcal{Q} \leq \max(\mathcal{Q}_1, \mathcal{Q}_2),$$

where $\mathcal{Q}_1$ and $\mathcal{Q}_2$ are given by

$$\mathcal{Q}_1 = \prod_{k=0}^{N^2-1} \left\{ (1-\varepsilon)a + a\left(\varepsilon - \frac{1}{28}\right)\left[\cos\left(\frac{2\pi k}{N^2}\right) + \cos\left(\frac{2\pi k}{N}\right)\right] \right.$$
$$-\frac{a}{28}\left[\cos\left(\frac{4\pi k}{N}\right) + \cos\left(\frac{6\pi k}{N}\right) + \cos\left(\frac{4\pi k}{N^2}\right)\right.$$
$$+\cos\left(\frac{6\pi k}{N^2}\right) + \cos\left(\frac{2\pi k(N+1)}{N^2}\right) + \cos\left(\frac{2\pi k(N+2)}{N^2}\right)$$
$$+\cos\left(\frac{2\pi k(N-1)}{N^2}\right) + \cos\left(\frac{2\pi k(N-2)}{N^2}\right) + \cos\left(\frac{2\pi k(2N+1)}{N^2}\right)$$
$$\left.\left.+\cos\left(\frac{2\pi k(2N+2)}{N^2}\right) + \cos\left(\frac{2\pi k(2N-1)}{N^2}\right) + \cos\left(\frac{2\pi k(2N-2)}{N^2}\right)\right]\right\} \tag{33}$$

and

$$\mathcal{Q}_2 = \prod_{k=0}^{N^2-1} \left\{ a(1-\varepsilon) + a\varepsilon\left[\cos\left(\frac{2\pi k}{N^2}\right) + \cos\left(\frac{2\pi k}{N}\right)\right]\right\}. \tag{34}$$

These two quantities allow us to delimit a region in the (a,ε) plane in which the Perron–Frobenius operator admits the cyclical spectral decomposition of Section 4.1. This region is obtained by applying the criterion (27) to the system (31) with $\mathcal{Q} = \mathcal{Q}_1$ and $\mathcal{Q} = \mathcal{Q}_2$. Define

$$\mathcal{Q}_u = \prod_{k=0}^{N^2-1} \lambda_k^{(u)}, \quad u = 1,2,$$

where the $\lambda_k^{(u)}$ are given implicitly in Eqs. (33) and (34).

5.3. *Calculating* $\sin\theta(\tilde{\pi})$

To determine the quantity $\sin\theta(\tilde{\pi})$, note that the phase space $\mathbb{X}$ of the transformation Φ defined in (31) is again the direct product $[0,1]^N$ if there are N elements on the lattice. On each of the intervals in $\mathbb{X}$, the transformation $S^{(i)}$ is strictly monotone on four segments $I_1 = [0,\tau_t^i)$, $I_2 = [\tau_t^i, 2\tau_t^i)$, $I_3 = [2\tau_t^i, \tau_t^i + 1/2)$, $I_4 = [\tau_t^i + 1/2, 1]$, and each of the 4^N elements of Π is of the form $\pi_{\boldsymbol{k}}(i) = I_1^{k_1}(i) \times I_2^{k_2}(i) \times I_3^{k_3}(i) \times I_4^{k_4}(i)$ where $\sum_j k_j = N$ (again "i" is the index denoting spatial position on the lattice). Clearly, this partition is no longer rectangular (cf. Fig. 13). Using the definition of the thresholds τ_t^i given by Eq. (32), when $p = 4$ (i.e. the coupling is diffusive in dimension two), and $d = 28$, the minimum angle of intersection of two edges of the elements of the image partition is, from (B.2)

$$\theta = \tan^{-1}\left[-\frac{1}{2}\left(\frac{12543[16(1+2\varepsilon) - 15\varepsilon^2]}{1792 - 53764\varepsilon + 50740\varepsilon}\right)\right]. \tag{35}$$

From Appendix A, $\sin\theta(\tilde{\pi})$ can then be computed as in the linear coupling case (24). Hence, for the nonlinearly coupled CML (31), the condition (21) yields two criteria which give an estimate for the parameter space location of the transition from statistical stability to statistical periodicity:

$$\mathcal{Q}_u\left[1 + \frac{1}{\sin\theta(\tilde{\pi})}\right] < 1, \quad u = 1,2. \tag{36}$$

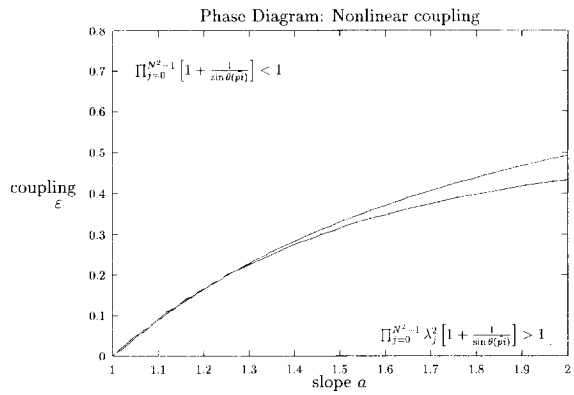

Fig. 11. Phase diagram for the nonlinearly coupled CML (31). The two curves displayed here are each obtained from (36) and they delimit a region which separates the (a, ε) plane in two: Above this region (in the upper left corner) the Perron–Frobenius operator for the CML admits a cyclical spectral decomposition as in (13). See text for details.

The two conditions in (36) delimit a transition region in the (a, ε) plane which separates two "phases". In one of them, there are sufficient conditions to guarantee a cyclical spectral decomposition of the Perron–Frobenius operator. Fig. 11 displays the "fuzzy" phase diagram resulting from the application of the two conditions in (36) to the system (1) with (31).

6. Discussion

The probabilistic description of CML's presented here is a first step towards a more complete understanding of the thermodynamics and statistical mechanics of these models. For example, comparing Figs. 8 and 9 confirms (for tent maps) the intuitive notion that systems with mean field coupling tend to order more easily than systems with short range interactions.

Although in some CML's there is a relationship between asymptotic periodicity and pattern formation, it is clear that this relationship is not absolute. Our findings can be summarized in the following way: For the systems discussed in this paper, asymptotic periodicity seems to be necessary for the formation of patterns in coupled lattices of chaotic maps.

The importance of the possible presence of statistical cycling in CML's and in more general spatially extended systems lies in its implications for the proper interpretation of the behavior of statistical descriptors of the motion: The notion of thermodynamic equilibrium for these objects must be extended to include a set of states visited sequentially in time.

The cycling of f_t observed for asymptotically periodic systems is an *ensemble property* and the classical statistical mechanics paradigm which associates a single invariant measure with the state of thermodynamic equilibrium does not apply here. Instead, the thermodynamic equilibrium of the asymptotically periodic CML consists in a sequence of states visited periodically in time. As demonstrated here, the CML's which possess this type of equilibrium are not "pathological" in the sense that they arise in the modeling of many physical and biological systems.

In addition, recognizing the presence of asymptotic periodicity is important for the proper interpretation of the law of large numbers as it applies to CML's. In fact, Pikovsky and Kurths [36] and Griniasty and Hakim [17] have started to explain the so-called "violations of the law of large numbers" reported by Kaneko [20] and Perez et al. in globally coupled CML's by pointing out that certain systems can be ergodic without being

mixing, and that in these cases, if the system is prepared out of equilibrium, it can converge (in the weak Cesàro sense) to an invariant density, while converging (in the weak sense) to a limit cycle (in density space). When this takes place, as is obviously the case for asymptotically periodic systems with $r > 1$ in (13), the ensemble statistics are no longer equivalent to the trajectory statistics, and since the law of large numbers refers to the convergence of *ensemble* statistics, it cannot be verified by investigating the properties of single trajectory statistics. While this argument is valid, Pikovsky and Kurths base their exposé on the reduction of the full Perron–Frobenius operator to a single "mean field" dimension, a reduction which is not possible in general when the coupling is local. The work we present here demonstrates that the full Perron–Frobenius operator can be shown analytically to be asymptotically periodic, and that future verifications of the law of large numbers in CML's should indeed focus on ensemble statistics, for local as well as long range coupling architectures.

The presence of statistical cycling also implies a type of dependence on the initial conditions which is much stronger than that usually discussed in reference to chaotic dynamical systems. Here the ensemble statistics depend on the initial ensemble. This is a consequence of the dependence of the functionals Γ_i on the initial density f_0 in Eq. (13) (cf. Remark 1 of Section 3.1).

The regions of parameter space in which asymptotic periodicity occurs are large (in a measure-theoretic sense) for all the systems discussed here. Therefore, the observation that the statistical quantifiers of the motion cannot be effectively calculated with respect to an invariant measure which exists (since the system can be ergodic) but which is almost never observed experimentally is ubiquitous for these CML's and not the result of very special circumstances.

It is interesting to note that the biologically important excitable CML's (Section 2) appear to belong to the class of CML's in which pattern formation and asymptotic periodicity are closely related. Since most realistic models of biological or physical relevance must include stochastic perturbations, we conclude by pointing out that analytic investigations of the transfer operator $\mathcal{P}_\Phi$ for stochastically perturbed CML's using appropriate techniques should generalize the approach presented here to a much broader class of spatially extended systems.

Acknowledgement

The authors wish to thank Rob Milson (Mathematics, McGill) for fruitful discussions. J.L. acknowledges support from the Fonds FCAR. This research was supported by grants from the National Institutes of Health (NIMH) and the North Atlantic Treaty Organization (NATO), the Natural Sciences and Engineering Research Council (NSERC) of Canada, and the Alexander von Humboldt Stiftung.

Appendix A

In this Appendix, we rigorously define and calculate the quantity $\sin\theta(\tilde{\pi})$ which appears in condition (21).

Since the partition $\Pi = \{\pi_i\}_{i=1}^{s}(\Pi)$ of $\mathbb{X} \subset \mathbb{R}^N$ is defined such that the restriction of Φ to π_i, denoted $\Phi_{|\pi_i}$, is differentiable and the π_i's are closed bounded (i.e. compact) domains having piecewise hyperplanar boundaries of finite $(N-1)$-dimensional measure, the angle at which edges of the π_i's intersect is bounded away from zero. In all the cases considered analytically, Φ is also piecewise linear. Hence the edges of the sets $\tilde{\pi}_i$ of the image partition $\tilde{\Pi}$ which are of positive measure also intersect at angles bounded away from zero, because the images of a hyperplane under the action of a piecewise linear Φ are (piecewise) hyperplanar.

Before proceeding with the analysis, it is useful to remind the reader with the concept of a regular cone in $\mathbb{R}^N$:

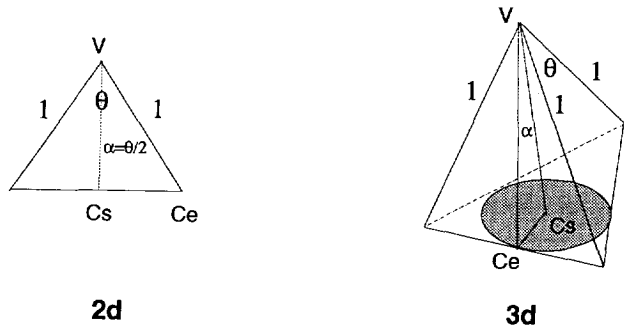

Fig. A.1. Illustration when $N = 2$ and $N = 3$ of the embedding of a $(N-1)$-sphere in a regular $(N-1)$-simplex (which is one face of a regular N-simplex). Cs denotes the centroid of the $(N-1)$-sphere, Ce denotes the centroid of one edge of the $(N-1)$-simplex containing the $(N-1)$-sphere. V denotes the vertex of the N-simplex not contained in the $(N-1)$-simplex.

Definition 3. Regular cone. A regular cone in $\mathbb{R}^N$ is a cone whose base is an $(N-1)$ dimensional disk d and such that the line joining the center of d to the apex V (not to be confused with the symbol $\bigvee$ used in Section 3 to denote the variation) of the cone is perpendicular to d. The angle between this central axis and any segment linking the apex of the cone to d's boundary is called the *summit angle.*

The apex of the cone V occurs at the singularities of derivative of Φ. Let $\mathrm{SP_i}$ be the set of all singular points of $\partial\pi_i$; hence if $\boldsymbol{x} \in \mathrm{SP_i}$,

$$\frac{\partial(\partial\pi_i(\boldsymbol{x}))}{\partial x_k} \quad \text{is not defined for some } k.$$

Construct at any $V_i \in \mathrm{SP_i}$ the largest possible regular cone having its apex at V_i and lying completely in π_i. Denote the summit angle of this cone by $\alpha(V_i)$. Now let

$$\alpha(\theta_{\pi_i}) = \min_{V_i \in \mathrm{SP_i}} \alpha(V_i) = \alpha(V)$$

and define

$$\sin\theta(\tilde{\pi}_i) = |\sin(\alpha(\pi_i))|.$$

Finally, let

$$\sin\theta(\tilde{\pi}) \equiv \min_{\pi_i \in \Pi} \sin\theta(\tilde{\pi}_i).$$

Calculating $\sin\theta(\tilde{\pi})$ turns out to be straightforward when the π_i's are bounded by hyperplanes such that the edges of $\partial\pi_i$ intersecting at V_i do so with angle θ_{int}. To illustrate the procedure, consider Fig. 12 which illustrates the situation in $\mathbb{R}^2$ and $\mathbb{R}^3$. If $\mathrm{dist}(\boldsymbol{x}, \boldsymbol{y})$ denotes the Euclidean distance between points $\boldsymbol{x}$ and $\boldsymbol{y}$,

$$\sin\theta(\tilde{\pi}) = \frac{\mathrm{dist(Cs, Ce)}}{\mathrm{dist(V, Ce)}}, \tag{A.1}$$

where Cs is the center of the shaded circle, Ce the middle of one (and any) of the edges of the base of the "pyramid", and V is the apex of the regular cone. Note that if $\theta_{\mathrm{int}} = \pi/2$, then it is straightforward from the right of Fig. 12 that $\sin\theta(\tilde{\pi}) = 1/\sqrt{3}$ in $\mathbb{R}^3$.

In $\mathbb{R}^N$, (A.1) holds when Cs is the centroid of the $(N-1)$-sphere embedded in one face of the regular N-simplex (which is a regular $(N-1)$-simplex), and Ce is the center of one of the edges of that $(N-1)$-simplex. Although it is not possible to draw the higher dimensional simpleces and spheres, it is easy to embed

them in an orthonormal reference frame and proceed with the analysis. For clarity, a simple case is considered before the more general result is given.

Case 1. $\tilde{\Pi}$ is a rectangular partition: $\theta_{\text{int}} = 90^0$ (warm up). In this case, any two adjacent edges of the N-simplex intersect at V with angle $\theta_{\text{int}} = \pi/2$. It is easy to show that in $\mathbb{R}^N$, if V is placed at the origin

$$\text{Cs} = \left(\frac{1}{N}, \cdots, \frac{1}{N}\right), \quad \text{Ce} = \left(0, \frac{1}{N-1}, \cdots, \frac{1}{N-1}\right)$$

and therefore

$$\text{dist(Cs,Ce)} = \frac{1}{\sqrt{N(N-1)}}, \ \text{dist(V,Ce)} = \frac{1}{\sqrt{(N-1)}}$$

which implies that for a rectangular partition in $\mathbb{R}^N$,

$$\sin\theta(\tilde{\pi}) = \frac{1}{\sqrt{N}}. \tag{A.2}$$

Case 2. $\tilde{\Pi}$ is not a rectangular partition: θ_{int} arbitrary. In this case we still assume that any two adjacent edges of the N-simplex intersect at V with an arbitrary angle $\theta_{\text{int}} < \pi/2$, where θ_{int} is the same for all angles. The N vertices $v_1, \cdots, v_N$ of the $(N-1)$-simplex forming the base of the N-simplex having apex V at the origin have coordinates which are cyclical permutations of each other. Thus, if $v_1 : (\kappa_1, \cdots, \kappa_N)$, then $v_i : (\text{Per}^i\{\kappa_1, \cdots, \kappa_N\})$ where $\text{Per}\{\kappa_1, \cdots, \kappa_N\} = \{\kappa_N, \kappa_1, \cdots, \kappa_{N-1}\}$. Therefore,

$$\text{Cs} = \left(\frac{\sum_{i=1}^N \kappa_i}{N}, \cdots, \frac{\sum_{i=1}^N \kappa_i}{N}\right), \quad \text{Ce} = \left(\frac{\sum_{i=2}^N \kappa_i}{N-1}, \cdots, \frac{\sum_{\substack{i=1 \\ i\neq j}}^N \kappa_i}{N-1}, \cdots, \frac{\sum_{i=1}^{N-1} \kappa_i}{N-1}\right)$$

which implies

$$\sin\theta(\tilde{\pi}) = \frac{1}{N}\sqrt{\frac{\sum_{j=1}^N \left(N\kappa_j - \sum_{i=1}^N \kappa_i\right)^2}{\sum_{j=1}^N \left(\sum_{\substack{i=1 \\ i\neq j}}^N \kappa_i\right)^2}}. \tag{A.3}$$

Note that if all but one of the κ_i's are zero, and the nonzero κ_i is 1, the vertices v_i all lie on the N dimensional hypercube, and therefore the edges which bound $\partial\pi_i$ intersect at right angles: Π is rectangular as in case 1, and (A.3) yields $\sin\theta(\tilde{\pi}) = 1/\sqrt{N}$ as expected.

From a practical point of view, given an N dimensional lattice transformation, it is easy to construct the partition Π, but it can be time consuming to obtain the κ_i's used in (A.3). On the other hand, it is usually straightforward to compute, in terms of the parameters of the transformation, the smallest angle θ_{int} subtended by the edges of the π_i's. It is therefore useful to express $\sin\theta(\tilde{\pi})$ in terms of this θ_{int}. To do so, note that the N apexes v_i (with coordinates $\{\kappa_i\}$) of a N-simplex whose summit V is placed at the origin, and whose edges intersect there at angles θ_{int} all lie on lines which link the centroid Cs to the apexes of the N-simplex whose edges intersect at the origin at an angle $\pi/2$ (think of the 2 and 3 dimensional situations). The equation of one of these lines is, from our discussion of Case 1,

$$-\frac{\kappa_1 - 1}{1 - 1/N} = N\kappa_2 = \ldots = N\kappa_N, \tag{A.4}$$

and the equations for the $(N-1)$ other lines are obtained by permuting x_1 with the remaining $(N-1)$ coordinates in (A.4). In addition, all of the v_i's have to be equidistant from Cs. Therefore, we obtain a second set of constraints which must be satisfied by the κ_i's:

$$\left(\kappa_1 - \frac{1}{N}\right)^2 + \sum_{i=2}^{N}\left(\kappa_i - \frac{1}{N}\right)^2 = d_{csv}^2$$

or

$$\left(\kappa_1 - \frac{1}{N}\right)^2 + (N-1)\left(\frac{\kappa_1 - 1}{N-1} + \frac{1}{N}\right)^2 = d_{csv}^2, \tag{A.5}$$

where d_{csv} is the distance between Cs and the v_i's. Solving these equation yields, for apexes v_1 and v_2 for example,

$$v_1 = \left(\frac{1}{N} + d_{csv}\sqrt{\frac{N-1}{N}}, \frac{1}{N} - \frac{d_{csv}}{\sqrt{N(N-1)}}, \cdots, \frac{1}{N} - \frac{d_{csv}}{\sqrt{N(N-1)}}\right), \tag{A.6}$$

$$v_2 = \left(\frac{1}{N} - \frac{d_{csv}}{\sqrt{N(N-1)}}, \frac{1}{N} + d_{csv}\sqrt{\frac{N-1}{N}}, \cdots, \frac{1}{N} - \frac{d_{csv}}{\sqrt{N(N-1)}}\right). \tag{A.7}$$

Now consider vectors $\mathrm{V}\boldsymbol{v}_i$ and $\mathrm{V}\boldsymbol{v}_j$ where $i \neq j$. The angle subtended by these two vectors is θ_{int} by definition. Therefore,

$$\cos(\theta_{int}) = \frac{\mathrm{V}\boldsymbol{v}_i \cdot \mathrm{V}\boldsymbol{v}_j}{|\,\mathrm{V}\boldsymbol{v}_i\,||\,\mathrm{V}\boldsymbol{v}_j\,|}$$

from which it is easy to obtain

$$d_{csv} = \sqrt{\frac{[1-\cos\theta_{int}](N-1)}{N[(N-1)\cos\theta_{int}+1]}}. \tag{A.8}$$

Replacing (A.8) in (A.7) yields the coordinates of the v_i's as a function of the angle θ_{int}:

$$\kappa_1 = \frac{1}{N} + \frac{N}{N-1}\sqrt{\frac{1-\cos\theta_{int}}{(N-1)\cos\theta_{int}+1}}, \qquad \kappa_i = \frac{1}{N} - \frac{1}{N}\sqrt{\frac{1-\cos\theta_{int}}{(N-1)\cos\theta_{int}+1}} \quad \text{if } i = 2, \cdots, N. \tag{A.9}$$

Using these expressions in (A.3) yields, for a lattice of N elements

$$\sin\theta(\tilde{\pi}) = \sqrt{\frac{1-\cos\theta_{int}}{N[1+(N-2)\cos\theta_{int}]}}. \tag{A.10}$$

Note that if $N = 3$ (A.10) reduces to

$$\sin\theta(\tilde{\pi}) = \frac{1}{\sqrt{3}}\tan\left(\tfrac{1}{2}\theta_{int}\right)$$

which can be easily derived directly from Fig. A.1 using simple geometrical arguments.

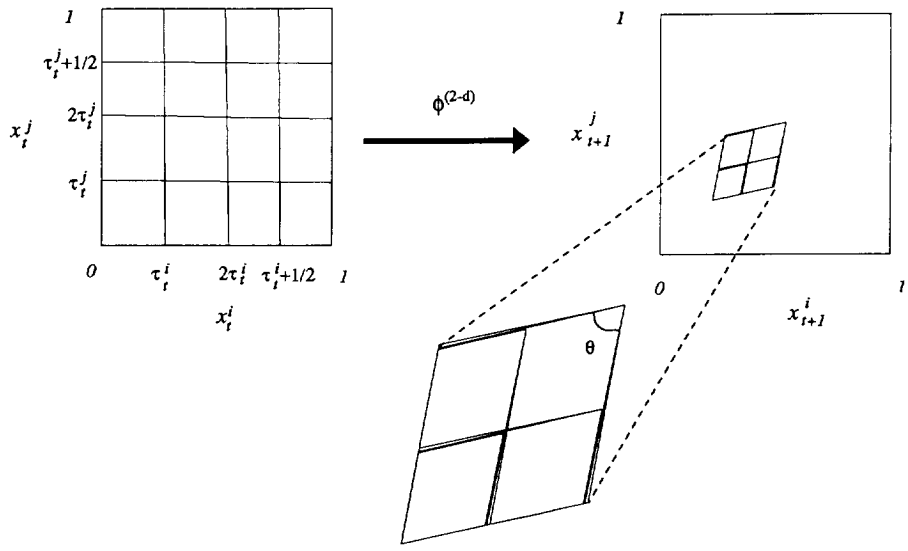

Fig. B.1. Illustration of the evolution of one face of the hypercube $\mathbb{X} = [0,1]^N$. On each of the rhomboids on the left panel, the transformation Φ is linear with slope $\pm a$. The panel on the right displays the images of these rhomboids. θ_{int} is the smallest angle formed by the edges of the "image rhomboids". In this figure, parameters are $a = 1.4$, $\varepsilon = 0.45$, $p = 28$, $d = 4, \overline{\tau}_t^i = \overline{\tau}_t^j = 0.15, \overline{x}_t^i = \overline{x}_t^j = 0.225$ (the symmetry was chosen for pedagogical purposes; it is in general not present for random initial conditions).This figure was computed with the symbolic manipulator MAPLE.

Appendix B

In this Appendix, the angle θ_{int} and the quantity $\sin\theta(\tilde{\pi})$ are computed explicitly for the coupled bimodal maps of Section 5.1. Fig. B.1 schematically illustrates the evolution of the unit square under the action of the transformation Φ defined in Section 5.1. Before proceeding, we introduce the following notation:

$$\overline{\tau}_t^i = \frac{1}{4p}\sum_{k\neq i,j} x_t^{(k)}, \quad k,j \in p \text{ - neighbourhood of } i,$$

$$\overline{x}_t^i = \frac{1}{d}\sum_{k\neq i,j} x_t^{(k)}, \quad k,j \in d \text{ - neighbourhood of } i,$$

Hence the two dimensional restriction $\Phi^{(2-d)}$ of the transformation Φ, which describes the evolution of one face of the hypercube $\mathbb{X}$ is given by:

$$\begin{aligned}\Phi^{(2-d)(i)}(\boldsymbol{x}_t) &= (1-\varepsilon)S^{(i)}(\boldsymbol{x}_t) + \frac{\varepsilon}{p}S^{(j)}(\boldsymbol{x}_t) + \overline{x}_t^i,\\ \Phi^{(2-d)(j)}(\boldsymbol{x}_t) &= (1-\varepsilon)S^{(j)}(\boldsymbol{x}_t) + \frac{\varepsilon}{p}S^{(i)}(\boldsymbol{x}_t) + \overline{x}_t^j\end{aligned} \tag{B.1}$$

where the local transformation is again given by (31).

Determining θ_{int} is straightforward but lengthy, and we have relied heavily on the use of a symbolic manipulator to carry out the explicit calculations. The plan of the algorithm to compute θ_{int} is as follows:

(1) Using the definition of $\Phi^{(2-d)}$, obtain the coordinates of the 25 vertices of the 16 rhomboids on which $\Phi^{(2-d)}$ is linear (these are displayed on the left panel of Fig. B.1).

(2) Iterate each of these points, so as to obtain 16 "image rhomboids" (displayed on the right of Fig. B.1).

(3) Using these coordinates, find the angles of intersection of the edges of these image rhomboids, and find the smallest one, which is by definition θ_{int}. Though the problem seems intractable at first glance, the task is greatly simplified by the many symmetries in the coordinates of the image rhombs, so that it is not necessary to perform a time-consuming minimization problem.

The analytic expression for θ_{int} is, as expected, independent of the slope a. It is given implicitly by

$$\tan\theta_{\text{int}} = -\frac{1}{2}\left\{\frac{(1-16d^2)[p^2(1-2\varepsilon)+\varepsilon^2(1-p^2)]}{4dp^2-\varepsilon p[1+8d(p+2d)]+\varepsilon^2[4d(1+p(1+4d))+p]}\right\}. \tag{B.2}$$

This expression can then be used in (A.10) of the previous appendix, to obtain an expression for the quantity $\sin\theta(\tilde{\pi})$ in terms of the control parameters of the CML of Section 5.1.

References

[1] R.E. Amritkar, P.M. Gade, A.D. Gangal and V.M. Nandkumaran, Stability of periodic orbits of coupled map lattices, Phys. Rev. Lett. 44 (1991) 3407–3410.
[2] C. Beck and F. Schlögl, Thermodynamics of Chaotic Systems (Cambridge Univ. Press, Cambridge, 1993).
[3] J.R. Beddington, Age distribution and the stability of simple discrete time population models, J. Theor. Biol. 47 (1974) 65–74.
[4] L.A. Bunimovich and Y.G. Sinai, Spacetime chaos in coupled map lattices, Nonlinearity 1 (1988) 491–516.
[5] L.A. Bunimovich and Y.G. Sinai, Statistical mechanics of coupled map lattices, in: Theory and Applications of Coupled Map Lattices, K. Kaneko, ed. (Wiley, 1993)pp. 169–189.
[6] H. Chaté and P. Manneville, Evidence of collective behavior in cellular automata, Europhys. Lett. 14 (1991) 409–413.
[7] H. Chaté and P. Manneville, Collective behaviors in spatially extended systems with local interactions and synchronous updating, Prog. Theor. Phys. 87 (1992) 1–60.
[8] H. Chaté and P. Manneville, Emergence of effective low dimensional dynamics in the macroscopic behavior of coupled map lattices, Europhys. Lett. 17 (1992) 291–296.
[9] C. Clark, Mathematical Bioeconomics: The Optimal Management of Renewable Resources (Wiley, Toronto, 1976) cf. pp. 230–232.
[10] G. Cocho, A.G. Santiago and G. Martínez-Mekler, An interplay between local and global dynamics in biological networks: The case of genetic sequences, in: NATO ASI Series C (Vol. 396): Cellular Automata and Cooperative Systems, N. Boccara E. Goles, S. Martínez and P. Picco, eds. (Kluwer, 1993)pp. 85–100.
[11] M. Cross and P. Hohenberg, Pattern formation outside of equilibrium, Rev. Mod. Phys. 65 (1993) 851–1086, we refer specifically to Section VII-D (pp. 950–953) of the review.
[12] M. Eigen and P. Schuster, The hypercycle (Springer, Berlin, 1979).
[13] J. Franke and A.A. Yakubu, Extinction in systems of bobwhite quail type populations, Can. Appl. Math. Quart. (1994), in press.
[14] J. Gallas P. Grassberger, H. Hermann and P. Ueberholz, Noisy collective behavior in cellular automata, Physica A 180 (1992) 19–41.
[15] E. Giusti, Minimal surfaces and functions of bounded variation (Birkhäuser, Berlin, 1984).
[16] P. Góra and A. Boyarski, Absolutely continous invariant measures for piecewise expanding C^2 transformations in $\mathbb{R}^n$, Isr. J. Math. 67 (1989) 272–285.
[17] M. Griniasty and V. Hakim, Correlation and dynamics in ensembles of maps: Simple models, Phys. Rev. E 49 (1994) 2661–2667.
[18] G. He and J. Li, The mechanism of pattern selection in coupled map lattices, Phys. Lett. A 185 (1994) 55–58.
[19] K. Kaneko, Period doubling of kink–antikink patterns, quasiperiodicity of antiferro-like structures and spatial intermittency in coupled logistic lattice – Toward a prelude of a field-theory of chaos, Prog. Theor. Phys. 72 (1984) 480–486.
[20] K. Kaneko, Globally coupled chaos violates the law of large numbers but not the Central-Limit Theorem, Phys. Rev. Lett. 65 (1990) 1391–1394.
[21] K. Kaneko, Supertransients, spatiotemporal intermittency and stability of spatiotemporal chaos, Phys. Lett. A 149 (1990) 105–112.
[22] K. Kaneko, Mean field fluctuations of a network of chaotic elements, Physica D 55 (1992) 368–384.
[23] J. Komornik, Asymptotic periodicity of the iterates of weakly contrictive Markov operators, Tohoku Math. J. 38 (1986) 15–27.
[24] J. Komornìk and A. Lasota, Asymptotic decomposition of Markov operators, Bull. Polish Acad. Sci. 35 (1987) 321–327.
[25] A. Lasota and M.C. Mackey, Chaos, Fractals and Noise: Stochastic Aspects of Dynamics (Springer, New York, 1994).
[26] H. Levine and W. Reynolds, Coupled map lattice techniques for simulating interfacial phenomena in reaction–diffusion systems, Chaos 2 (1992) 337–342.
[27] J. Losson and M.C. Mackey, Statistical cycling in coupled map lattices, Phys. Rev. E 50 (1994) 843–856.
[28] J. Losson and M. Mackey, Statistical cyling in two diffusively coupled maps, Physica D 72 (1994) 324–342.
[29] M.C. Mackey, Time's Arrow: The Origin of Thermodynamic Behavior (Springer, Berlin, 1992).
[30] B. McCoy and T. Wu, The Two-Dimensional Ising Model, (Harvard Univ. Press, Cambridge, MA, 1973).

[31] J. Milton and J. Bélair, Chaos, noise and extinction in models of population growth, Theor. Pop. Biol. 37 (1990) 273–290.
[32] T. Muir, A Treatise on the Theory of Determinants (Dover, New York, NY, 1960).
[33] H. Nozawa, A neural network model as a globally coupled map and applications based on chaos, Chaos 2 (1992) 377–386.
[34] G. Perez, S. Sinha and A. Cerdeira, Order in the turbulent phase of globally coupled maps, Physica D 63(1993) 341–349.
[35] A. Pikovsky, A dynamical model for periodic and chaotic oscillations in the Belousov–Zhabotinskii reaction, Phys. Lett. A 85 (1981) 13–16.
[36] A. Pikovsky, Do globally coupled maps really violate the law of large numbers, Phys. Rev. Lett. 72 (1994) 1644–1646.
[37] C. Price, P. Wambacq and A. Oosterlinck, The plastic coupled map lattice: A novel image-processing paradigm, Chaos 2 (1992) 351–366.
[38] A. Shrier, H. Dubarsky, M. Rosengarten, M.R. Guevarra, S. Nattel and L. Glass, Prediction of complex atrioventricular conduction rhythms in humans with use of the atrio-ventricular nodal recovery curve, Circulation 76 (1987) 1196–1205.
[39] R. Solé and J. Valls, On structural stability and chaos in biological systems, J. Theor. Biol 155 (1992) 87–102.
[40] C.T. Ionescu-Tulcea and G. Marinescu, Théorie ergodique pour des classes d'opérations non complètement continues, Ann. Math. 52 (1950) 140–147.
[41] T. Yoshida, H. Mori and H. Shigematsu, Analytic study of chaos of the tent map: Band structures, power spectra and critical behaviors, J. Stat. Phys. 31 (1983) 279.